Supplementary Information

Electronic properties of double-atom catalysts for electrocatalytic oxygen evolution reaction in alkaline: A DFT study

Chunhua Yang [a], Yang Wu [a], Yuxiu Wang [b], He-Na Zhang [a], Liang-Hui Zhu [a], Xiao-Chun Wang [a,*]

[a] *Institute of Atomic and Molecular Physics, Jilin University, Changchun, 130012, P.R. China*

[b] *Department of Ecology and Environment, Yuzhang Normal University, Nanchang, 330103, P.R. China*

* *Corresponding Author.* wangxiaochun@jlu.edu.cn

Calculation details

1. Formation energy (E_f), binding energy (E_b) and cohesive energy (E_{coh})

In order to adopt the optimal coordination configurations of the 2TM embedded in nitrogen-decorative graphene, the formation energy (E_f) of 2TM-NG was calculated by using the Eq. s1 [S1,S2]:

$$E_f = E_{2TM\text{-}NG} + 10\square c - (E_{Gra} + 6\mu_N + \mu_{TM1} + \mu_{TM2}) \quad \text{(Eq. s1)}$$

where $E_{2TM\text{-}NG}$ is the total energy of 2TM-NG, E_{Gra} is the total energy of the pristine 7×7 graphene supercell and μ_C is the chemical potential of C atom [S3,S4], and μ_N is the chemical potential of N atom taken from a N_2 molecule in the gas phase [S5]. μ_{TM1} and μ_{TM2} are the chemical potentials of transition metals (Fe/Co/Ni in its bcc/hcp/fcc bulk structures, respectively) [S6].

In order to prove that the $N_{PA}G$ and N_PG can exhibit higher chemical activity and trap 2TM (FeCo, FeNi, CoNi), the binding energy (E_b) between the 2TM and the substrate was studied and defined as Eq. s2 [S7]:

$$E_b = E_{2TM\text{-}NG} - E_{NG} - E_{TM1} - E_{TM2} \quad \text{(Eq. s2)}$$

where $E_{2TM\text{-}NG}$ and E_{NG} represent the total energy of 2TM-NG and NG, respectively. E_{TM1} and E_{TM2} is the electronic energy of isolated transition metal atom (Fe, Co or Ni), and a lattice constant of 17.15 Å × 17.15 Å × 18.00 Å was used for this computation.

Due to the large cohesive energy (E_{coh}) of TM bulk, the feasibility of atomically dispersed 2TM-NG catalysts need to be further assessed [S8].

$$E_{coh} = E_{bulk} / n - E_{TM} \quad \text{(Eq. s3)}$$

where E_{bulk} is the energy of TM bulk, n is the number of atoms in the bulk, E_{TM} is the energy of free TM.

2. Gibbs free energy

The four elementary steps for OER process under alkaline conditions are shown in Eq (1-4). The Gibbs free energies ΔG_{OH*}, ΔG_{O*} and ΔG_{OOH*}, which correspond to OH*, O* and OOH* adsorption on the electrocatalyst models, were calculated according to Eq. s4 [S9]:

$$\Delta G_{ads} = \Delta E_{ads} + \Delta E_{ZPE} - T\Delta S_{ads} - \Delta G_U \quad \text{(Eq. s4)}$$

where ΔE_{ads} is the electronic adsorption energy, ΔE_{ZPE} is the zero-energy calculated from the vibrational frequencies, ΔS_{ads} is the entropy change, and T is the system temperature (298.15 K). ΔG_U = neU, where n is the number of transferred electrons, e is the elementary charge, and U is the electrode potential referenced to computational hydrogen electrode (CHE) model. At equilibrium potential U_0, some of the OER steps become uphill and an applied potential U is needed to surmount the positive free energy change. Thus, the over-potential is determined as $\eta = U - U_0$.

The free energy of $H_2O(l)$ derived as $G_{H2O(l)} = G_{H2O(g)} + RTln(p/p_0)$ since only $G_{H2O(g)}$ can be directly obtained by DFT calculations, where R is the ideal gas constant, T = 298.15 K, p = 0.035 bar, and p_0 = 1 bar. The free energy of OH^- was derived as $G_{OH^-} = G_{H2O(l)} - G_{H+}$, where $G_{H+} = 1/2G_{H2} - k_BTln10\times pH$ (k_B is Boltzmann's constant). Hence, the equilibrium potential U_0 for OER at pH = 14 was determined to be 0.402 V vs NHE according to the Nernst equation, where the reactant and product are at the same energy level [S10].

Since it is difficult to obtain the exact free energy of OH, O and OOH radicals in the electrolyte solution, the Gibbs free energies ΔG_{OH*}, ΔG_{O*} and ΔG_{OOH*} are defined as Eq. s5-s10:

$$\Delta G_{OH*} = (G_{OH*}) - (G_* + G_{OH^-}) \quad \text{(Eq. s5)}$$

$$\Delta G_{O*} = (G_{O*} + G_{H2O(l)}) - (G_* + 2G_{OH^-}) \quad \text{(Eq. s6)}$$

$$\Delta G_{OOH*} = (G_{OOH*} + G_{H2O(l)}) - (G_* + 3G_{OH^-}) \quad \text{(Eq. s7)}$$

$$\Delta G_{OH*}(U) = \Delta G_{OH*} - eU \quad \text{(Eq. s8)}$$

$$\Delta G_{O*}(U) = \Delta G_{O*} - 2eU \quad \text{(Eq. s9)}$$

$$\Delta G_{OOH*}(U) = \Delta G_{OOH*} - 3eU \quad \text{(Eq. s10)}$$

Table S1 A summary of OER performance of dual transition metals nitrides

Electrocatalysts	Electrolyte	Overpotential @ 10 mA cm^{-2} (mV)	Tafel slope ($mV\ dec^{-1}$)	Reference
TiN@Ni_3N	0.1 M KOH	350	93.70	[S11]
$FeNi_3N$-NPs	1.0 M KOH	280	46.00	[S12]
Ni_3FeN	1.0 M KOH	223	40.00	[S13]
$FeNi_3N$/NF	1.0 M KOH	202	40.00	[S14]
MNCC4	1.0 M KOH	290	65.00	[S15]
Co-FeN@MWCNT	1.0 M KOH	290	32.00	[S16]
Ni_3FeN-NP	1.0 M KOH	241	59.00	[S17]
CoFe(3:1)-N	1.0 M KOH	200	42.44	[S18]
Ni_3FeN/r-GO	1.0 M KOH	270	54.00	[S19]
$Co_{0.5}Fe_{0.85}$NSs	1.0 M KOH	266	30.00	[S20]

Table S2 Solvation energy (E_{solv}) of catalytic reaction intermediates, η/vac and η/sol for the OER reactions of FeCo-NG and FeNi-NG.

		FeCo -$N_{PA}G$	**FeCo -N_PG**	**FeCo -N_PG-O**	**FeNi -$N_{PA}G$**	**FeNi -N_PG**	**FeNi -N_PG-O**
E_{solv} (eV)	**OH***	-0.04	0.06	0.17	-0.05	0.03	-0.16
	O*	-0.09	0.02	-0.21	-0.07	0.06	-0.23
	OOH*	-0.10	-0.13	-0.19	-0.11	-0.15	-0.23
η/vac (eV)		0.42	1.41	0.98	0.65	1.49	0.91
η/sol (eV)		0.31	1.26	1.00	0.61	1.28	0.91

Table S3 The amount electrons (|*e*|) of N atoms and nearby C atoms in NG and CoNi –NG. The amount of electron changes (Δ|*e*|) of N atoms and nearby C atoms when CoNi atoms embedded in NG.

		$N_{PA}G$	CoNi-$N_{PA}G$	N_PG	CoNi-N_PG
|*e*|	**N**	-5.56	-6.91	-6.69	-7.26
	C	5.43	4.83	6.99	5.67
Δ|*e*|	**N**	-1.35		-0.57	
	C	-0.60		-1.32	

Table S4 The oxidation states of Co/Ni atom of CoNi-NG catalysts. ΔG values of CoNi-NG catalysts at U= 0V.

		oxidation state of Co (|e|)	oxidation state of Ni (|e|)	ΔG @ U= 0V (eV)
CoNi-N_{PA}G	*	0.93	0.87	--
	OH*	1.16	0.86	0.25
	O*	1.21	0.87	0.55
	OOH*	1.11	0.87	0.71
CoNi-N_{PA}G -OH	*	1.16	0.86	--
	OH*	1.27	0.87	0.31
	O*	1.32	0.88	0.85
	OOH*	1.27	0.89	0.62
CoNi-N_{PA}G -O	*	1.21	0.87	--
	OH*	1.35	0.87	0.60
	O*	1.31	1.01	1.21
	OOH*	1.31	0.83	0.25
CoNi-N_{P}G	*	0.67	0.56	--
	OH*	0.92	0.82	-0.30
	O*	1.01	0.91	-0.32
	OOH*	0.91	0.81	1.83
CoNi-N_{P}G -OH	*	0.92	0.82	--
	OH*	1.11	0.83	-0.03
	O*	1.20	0.85	0.54
	OOH*	1.10	0.83	0.83
CoNi-N_{P}G -O	*	1.01	0.91	--
	OH*	1.16	0.91	0.47
	O*	1.23	0.97	0.64
	OOH*	1.14	0.92	0.78

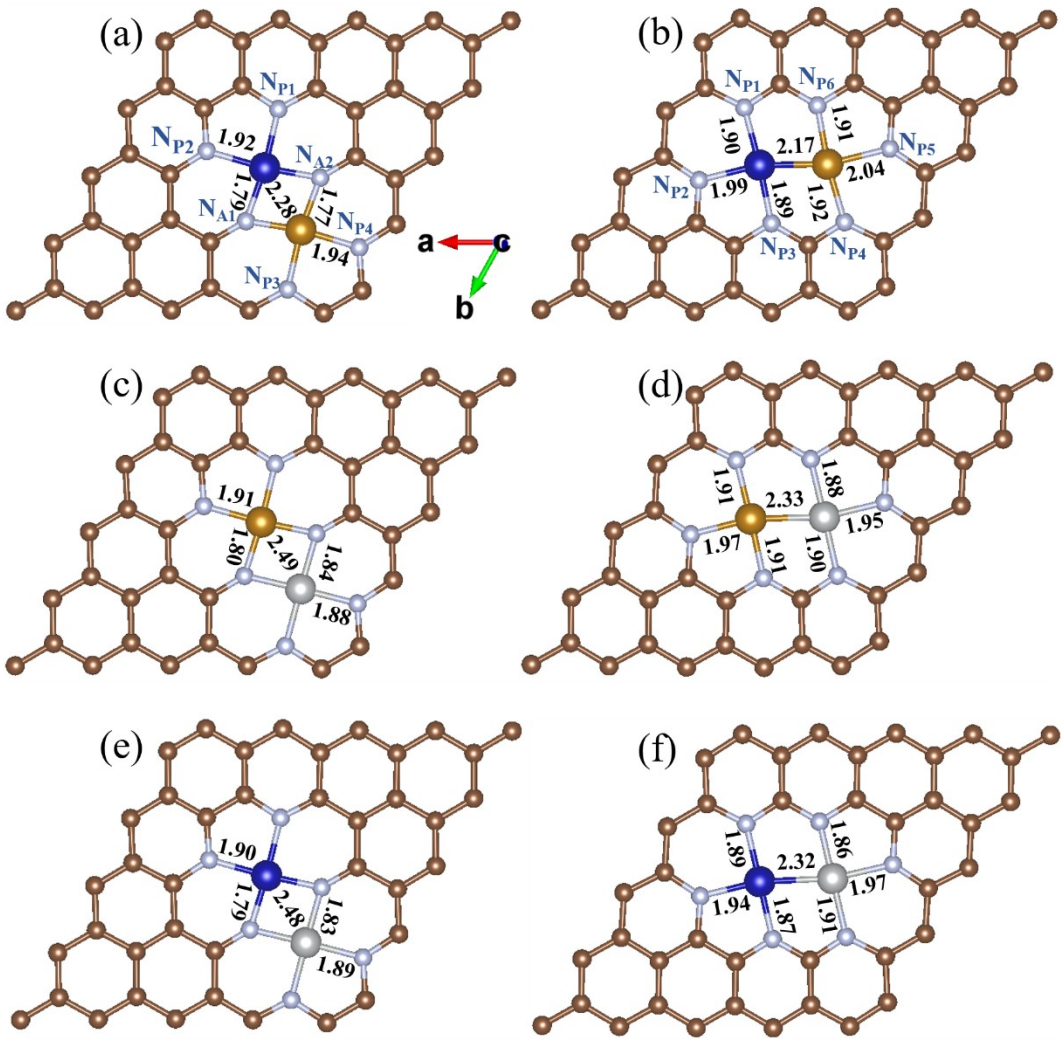

Fig. S1 The geometric structures and the mainly bonds lengths (Å) of (a) FeCo-N_{PA}G and (b) FeCo-N_{P}G; (c) FeNi-N_{PA}G and (d) FeNi-N_{P}G; (e) CoNi-N_{PA}G and (f) CoNi-N_{P}G. The golden, dark grey and blue balls represent Fe, Co and Ni atom, respectively.

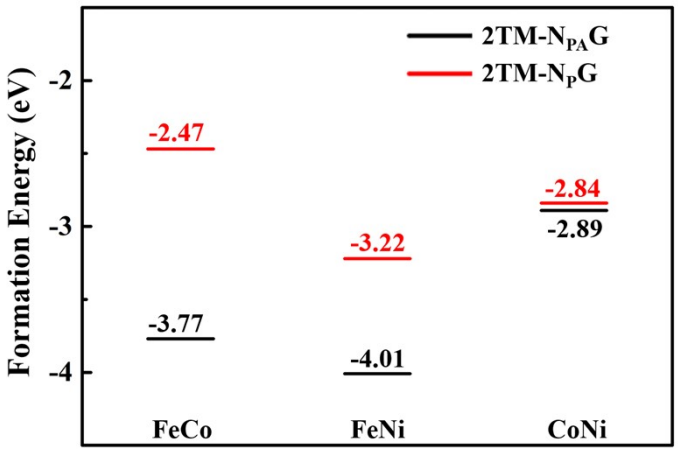

Fig. S2 The formation energy for 2TM-N$_{PA}$G and 2TM-N$_{P}$G**.**

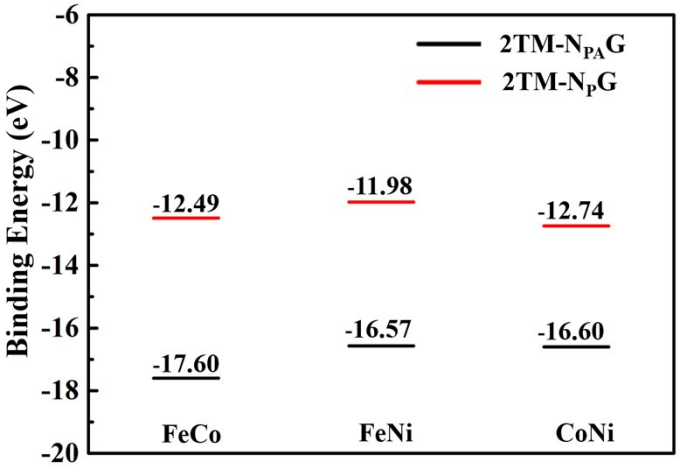

Fig. S3 The binding energy for 2TM-N$_{PA}$G and 2TM-N$_{P}$G.

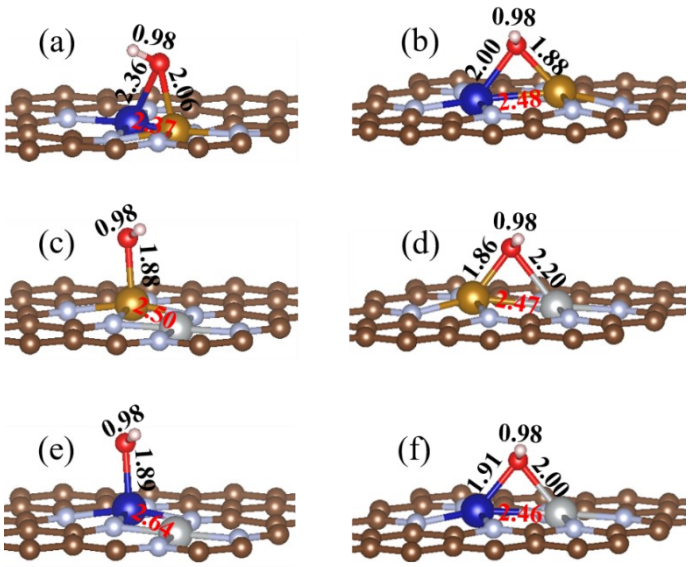

Fig. S4 OH radical adsorption configurations for (a) FeCo-$N_{PA}G$, (b) FeCo-$N_{P}G$, (c) FeNi-$N_{PA}G$, (d) FeNi-$N_{P}G$, (e) CoNi-$N_{PA}G$ and (f) CoNi-$N_{P}G$. The golden, dark grey and blue balls represent Fe, Co and Ni atoms, respectively.

For FeCo-$N_{PA}G$ and FeCo-$N_{P}G$ (Fig. S4 (a, b)), after adsorption of OH radical, the lengths of Fe-Co are 2.37 Å and 2.48 Å, respectively, and the lengths increased corresponding to that before adsorption. In addition, Fe-O and Co-O bonds with lengths of 2.06 Å, 2.36 Å (FeCo-$N_{PA}G$) and 1.88 Å, 2.00 Å (FeCo-$N_{P}G$) are formed. For FeNi-$N_{P}G$ and CoNi-$N_{P}G$ (Fig. S4 (d, f)), the adsorption configurations of OH radical are very similar to that of FeCo-$N_{P}G$. After OH radical is adsorbed in FeNi-$N_{PA}G$ (Fig. S4 (c)), the length of Fe-Ni is 2.50 Å. However, OH radical is only adsorbed on Fe site, and the calculated bond length between the Fe and O atoms is 1.88 Å, which is smaller than the length of Fe-O (2.06 Å) in FeCo-$N_{PA}G$. For CoNi-$N_{PA}G$ (Fig. S4 (e)), the Co-O bond length is 1.89 Å, and note that the bond length of Co-Ni is 2.64 Å, which is the longest TM1-TM2 bond length among these structures.

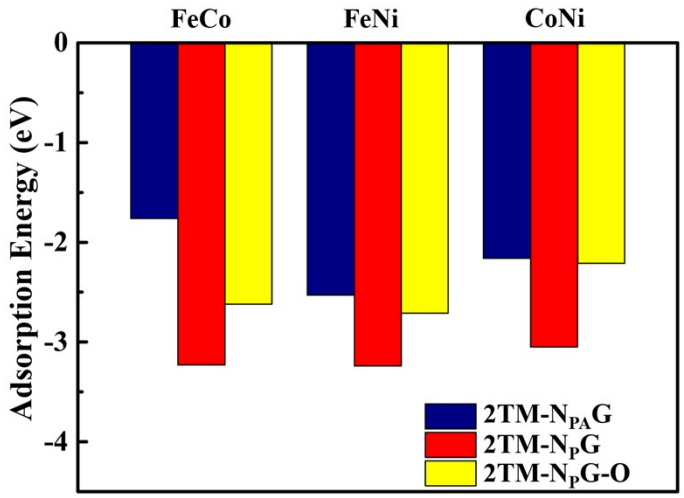

Fig. S5 OH radical adsorption energy for 2TM-$N_{PA}G$, 2TM-$N_{P}G$ and 2TM-$N_{P}G$-O.

To better judge the relative stability of OH radical adsorption on the catalysts surface, the adsorption energy (E_{ads}) is calculated as Eq. s11 [S1]:

$$E_{ads} = E_{OH*} - E(2TM\text{-}NG) - E_{OH} \quad \text{(Eq. s11)}$$

where E_{OH*} is the total energy of OH*, E(2TM-NG) and E_{OH} are the energies of 2TM-NG and OH radical (-7.14 eV). Negative adsorption energy indicates the exothermic process after OH radical adsorption on the substrate. The larger the negative value, the stronger the binding between OH radical and 2TM-NG [S21]. The E_{ads} of OH radical adsorbed on 2TM-$N_{P}G$ (-3.23 eV for FeCo, -3.24 eV for FeNi, -3.05 eV for CoNi) are lower than that adsorbed on 2TM-$N_{PA}G$ (-1.76 eV for FeCo, -2.53 eV for FeNi, -2.16 eV for CoNi) (Fig. S5), indicating that 2TM-$N_{P}G$ has higher adsorption activity and stability for OH radical.

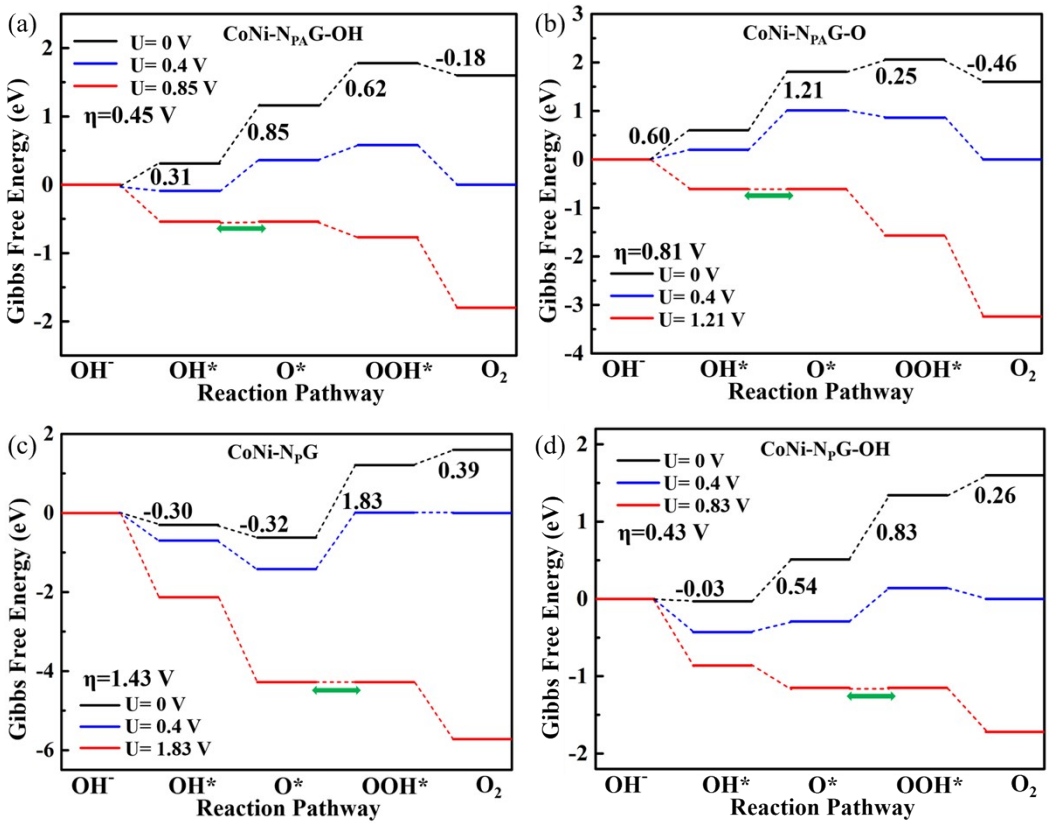

Fig. S6 At pH=14, the Gibbs free energy for the OER pathway for (a) CoNi-N_{PA}G-OH, (b) CoNi-N_{PA}G-O, (c) CoNi-N_PG and (d) CoNi-N_PG-OH.

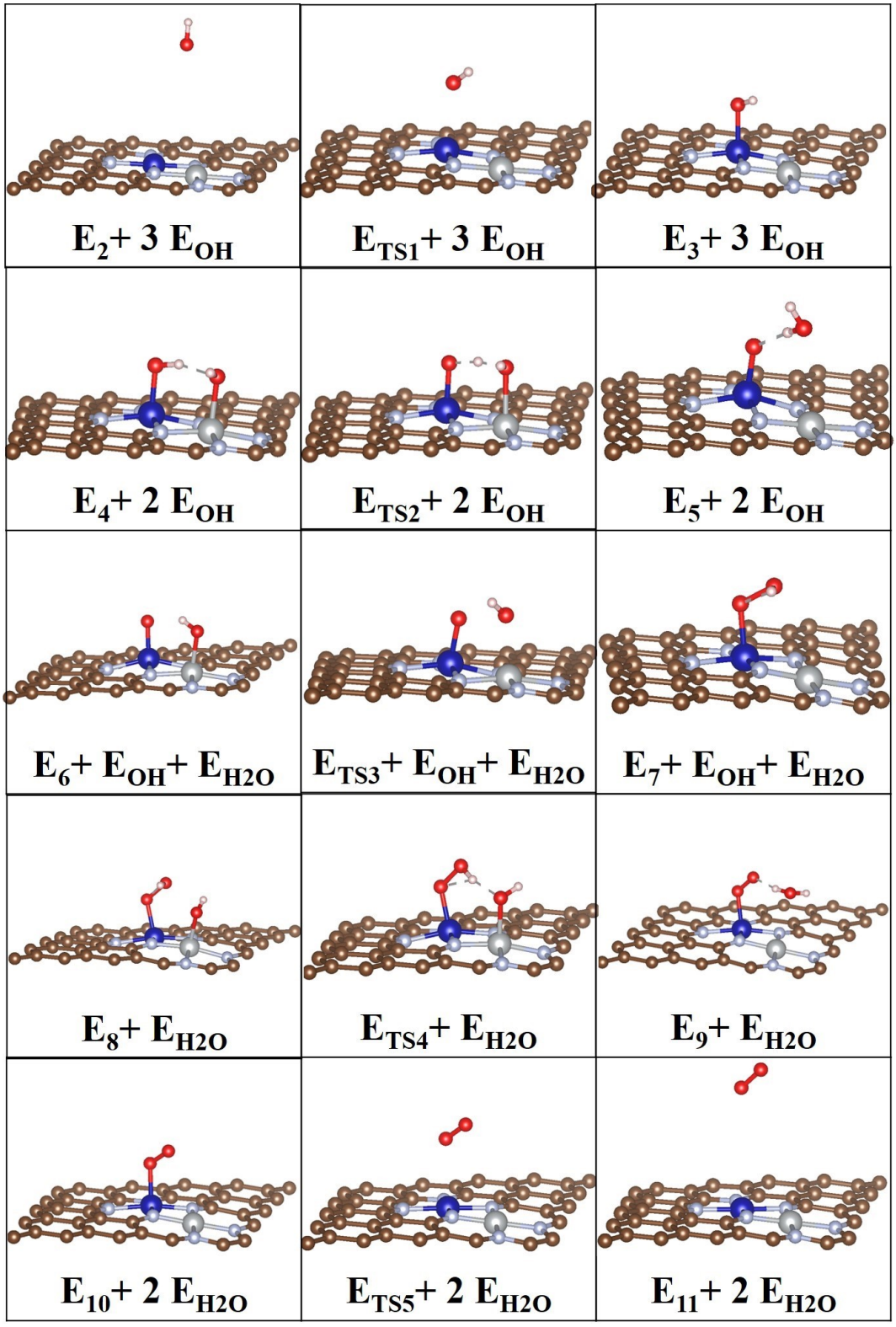

Fig. S7 Structures and energies corresponds to dynamic reaction pathway of OER for CoNi-$N_{PA}G$.

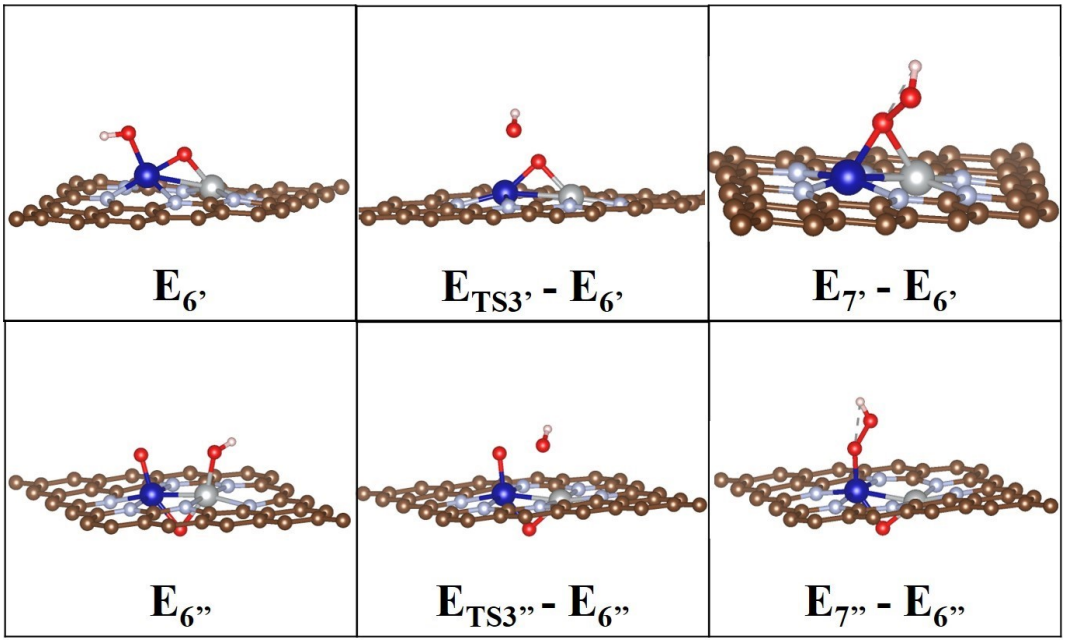

Fig. S8 Structures and energies corresponds to rate-determining step of OER for CoNi-N_PG (top) and CoNi-N_PG-O (bottom).

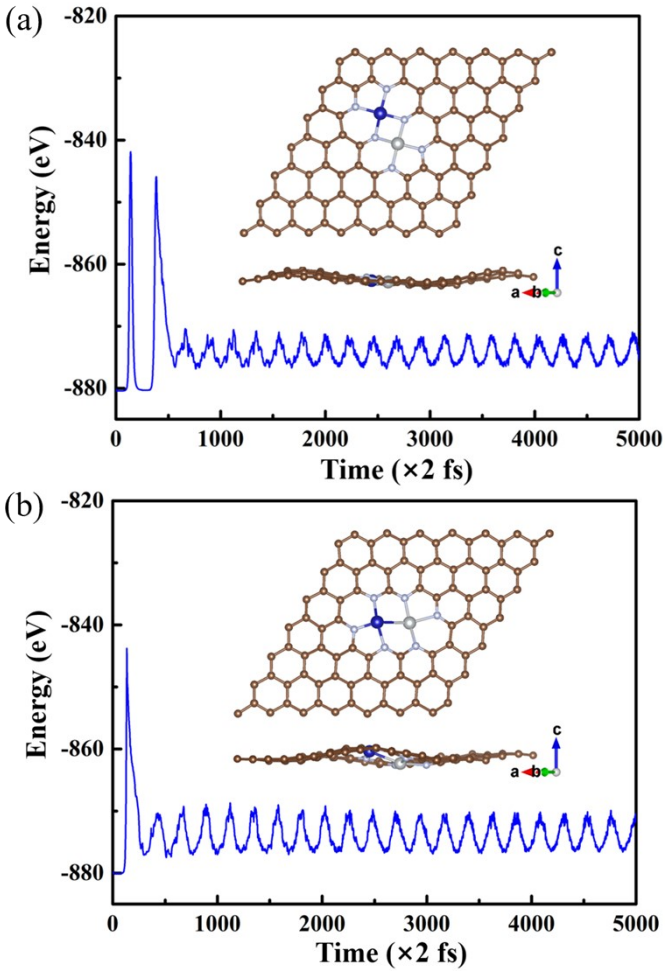

Fig. S9 Energy fluctuation of (a) CoNi-$N_{PA}G$, (b) CoNi-$N_{P}G$ during AIMD simulations at 500 K.

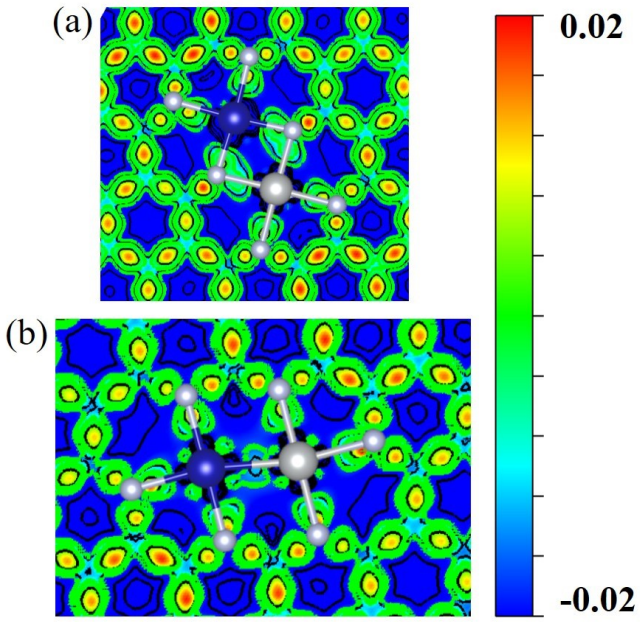

Fig. S10 The 2D charge density differences (differences between an interacting system and the superposition of atomic charge densities) for (a) CoNi-$N_{PA}G$ and (b) CoNi-N_PG. (The 2D charge density differences, which helps to visualize the characteristics of bonding, is defined as the differences between the CoNi-NG systems and the superposition of atomic charge densities, i.e., $\Delta\rho(r) = \rho(\text{CoNi-NG}) - \sum\rho(\text{atom})$.)

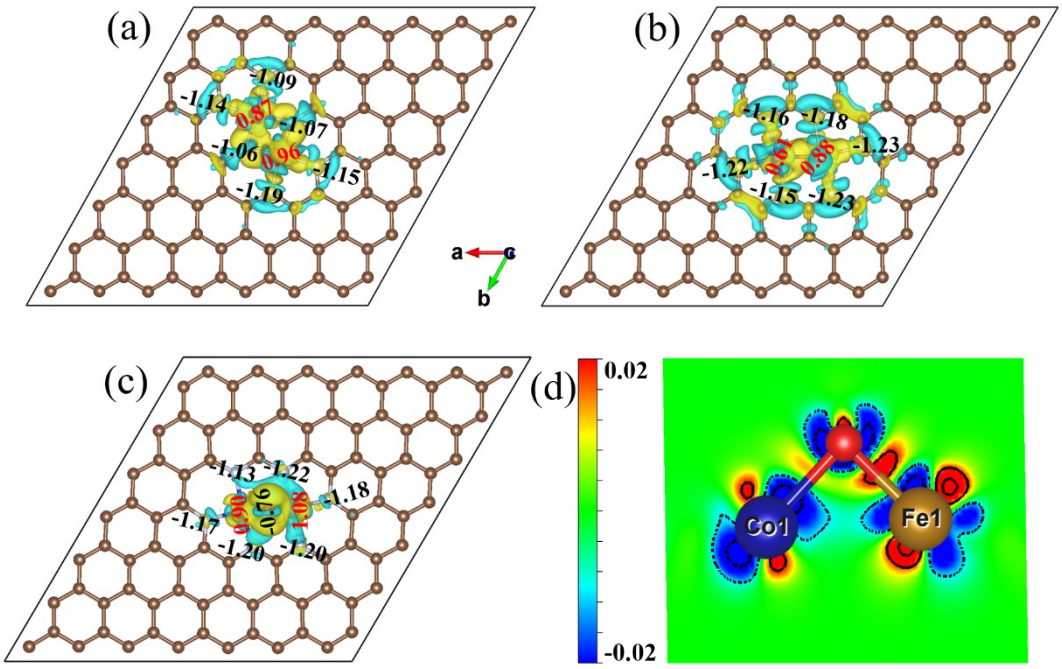

Fig. S11 The Bader charge analysis and the 3D charge density differences for (a) FeCo-$N_{PA}G$, (b) FeCo-N_PG, and (c) FeCo-N_PG-O. (d) The 2D plots clipping plane corresponding FeCo-N_PG-O crosses the three atoms of Co, O and Fe. Yellow (solid contour line) and blue (dashed contour line) correspond to accumulation and depletion of total valence electrons, respectively. The isosurface value is 0.0035 e $bohr^{-3}$.

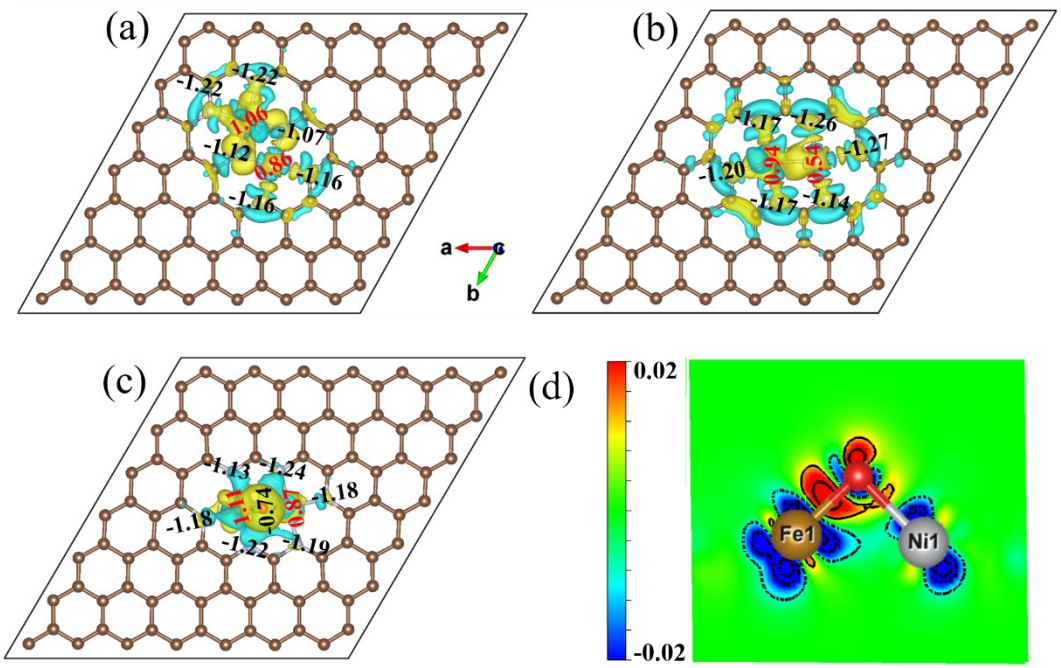

Fig. S12 The Bader charge analysis and the 3D charge density differences for (a) FeNi-N_PAG, (b) FeNi-N_PG, and (c) FeNi-N_PG-O. (d) The 2D plots clipping plane corresponding FeNi-N_PG-O crosses the three atoms of Fe, O and Ni. Yellow (solid contour line) and blue (dashed contour line) correspond to accumulation and depletion of total valence electrons, respectively. The isosurface value is 0.0035 e $bohr^{-3}$.

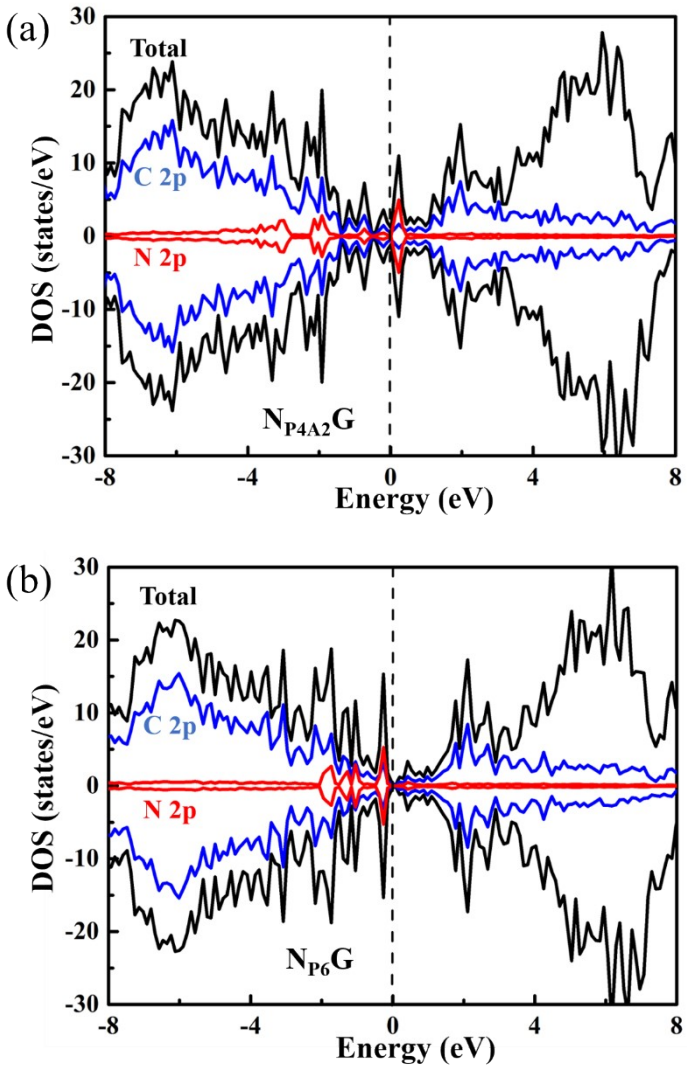

Fig. S13 Spin-polarized density of states for (a) $N_{PA}G$ and (b) $N_{P}G$.

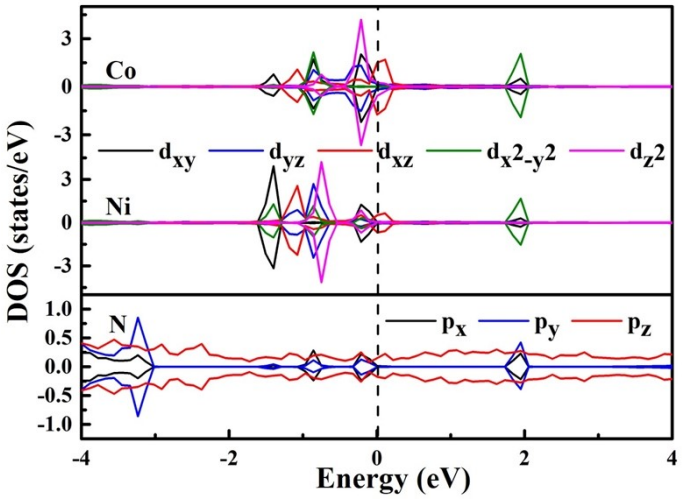

Fig. S14 Density of states of Co/Ni 3d and N 2p split orbitals for CoNi-$N_{P}G$.

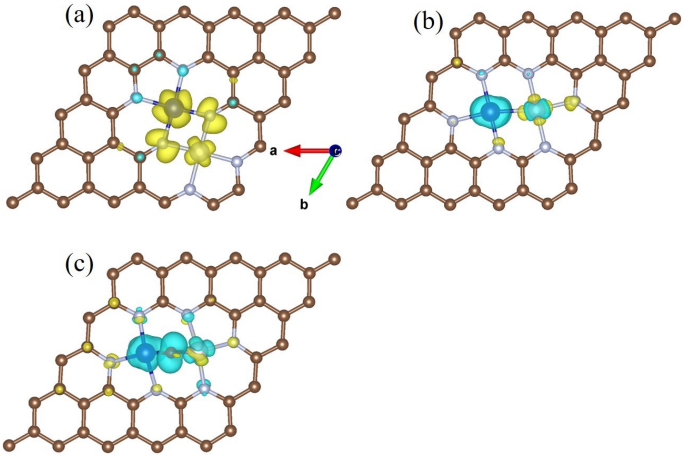

Fig. S15 Spin charge density of (a) CoNi-$N_{PA}G$, (b) CoNi-N_PG and (c) CoNi-N_PG-O.

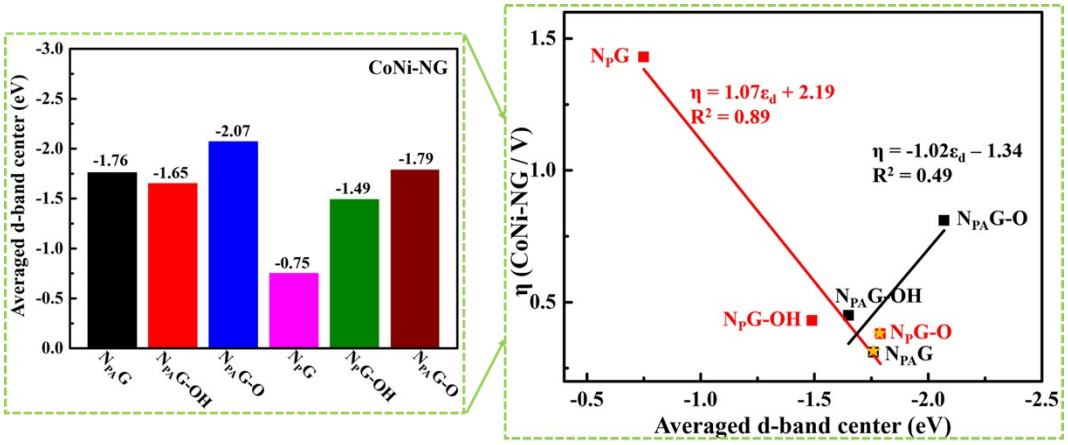

Fig. S16 Corresponding values and the correlation between over-potential (η) of CoNi-NG and the averaged d-band center (ε_d) for dual transition metal atoms (CoNi).

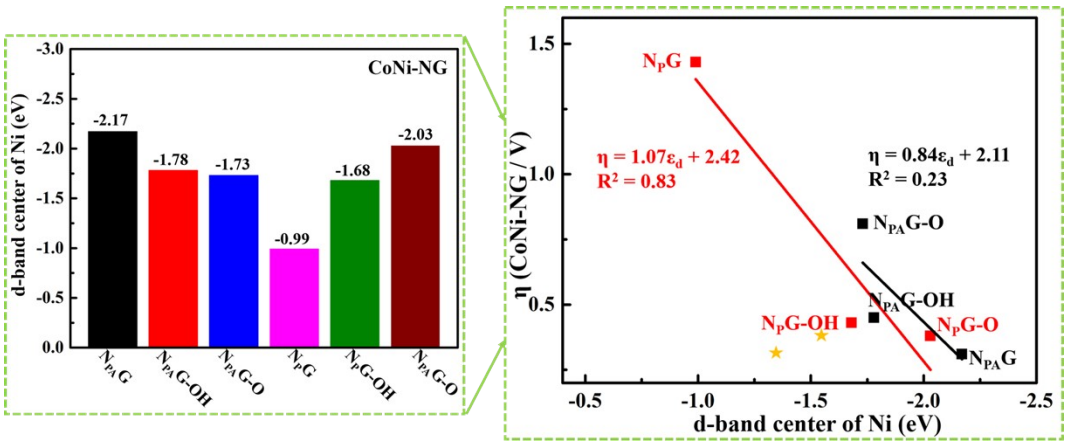

Fig. S17 Corresponding values and the correlation between over-potential (η) of CoNi-NG and d-band center (ε_d) of Ni atom.

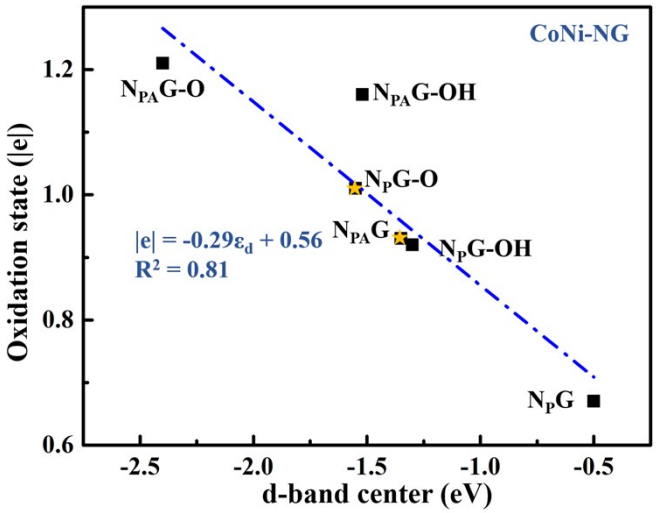

Fig. S18 Correlation between the oxidation state and d-band center (ε_d) of Co atom in CoNi-NG.

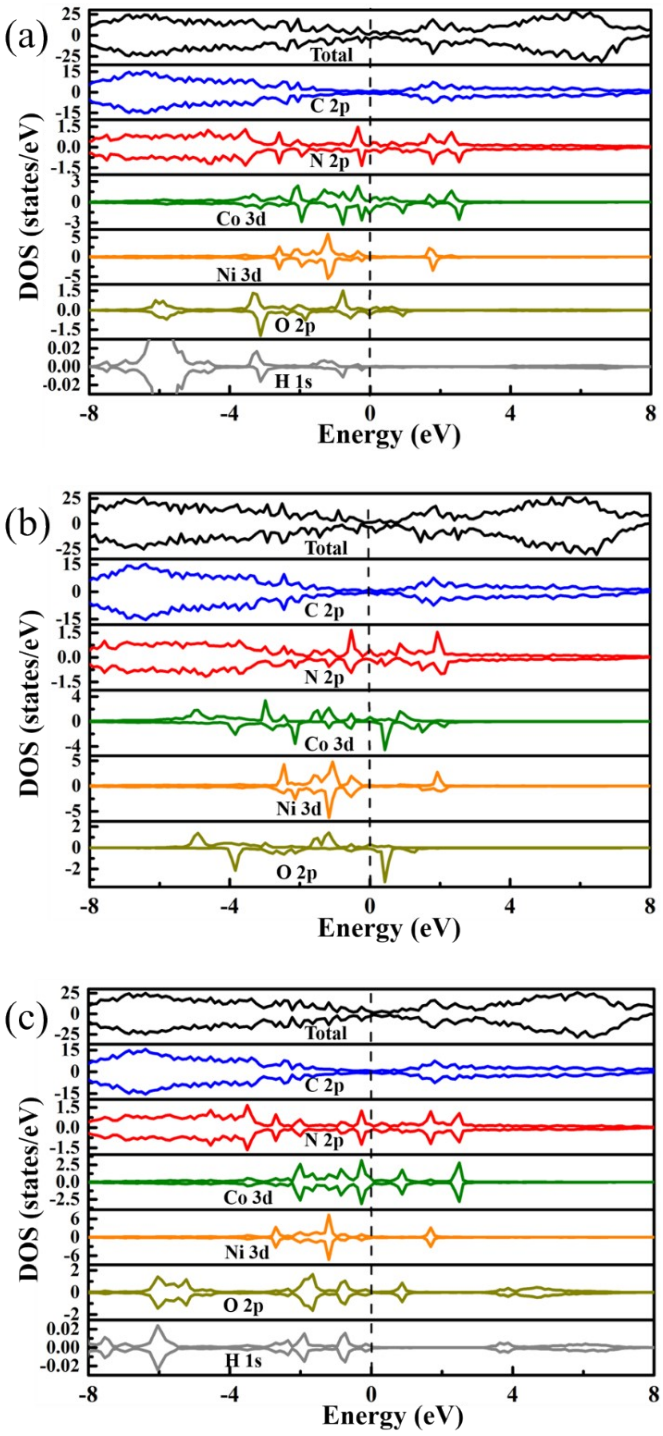

Fig. S19 Spin-polarized density of states for adsorption intermediates (a) OH*, (b) O*, and (c) OOH* on CoNi-$N_{PA}G$.

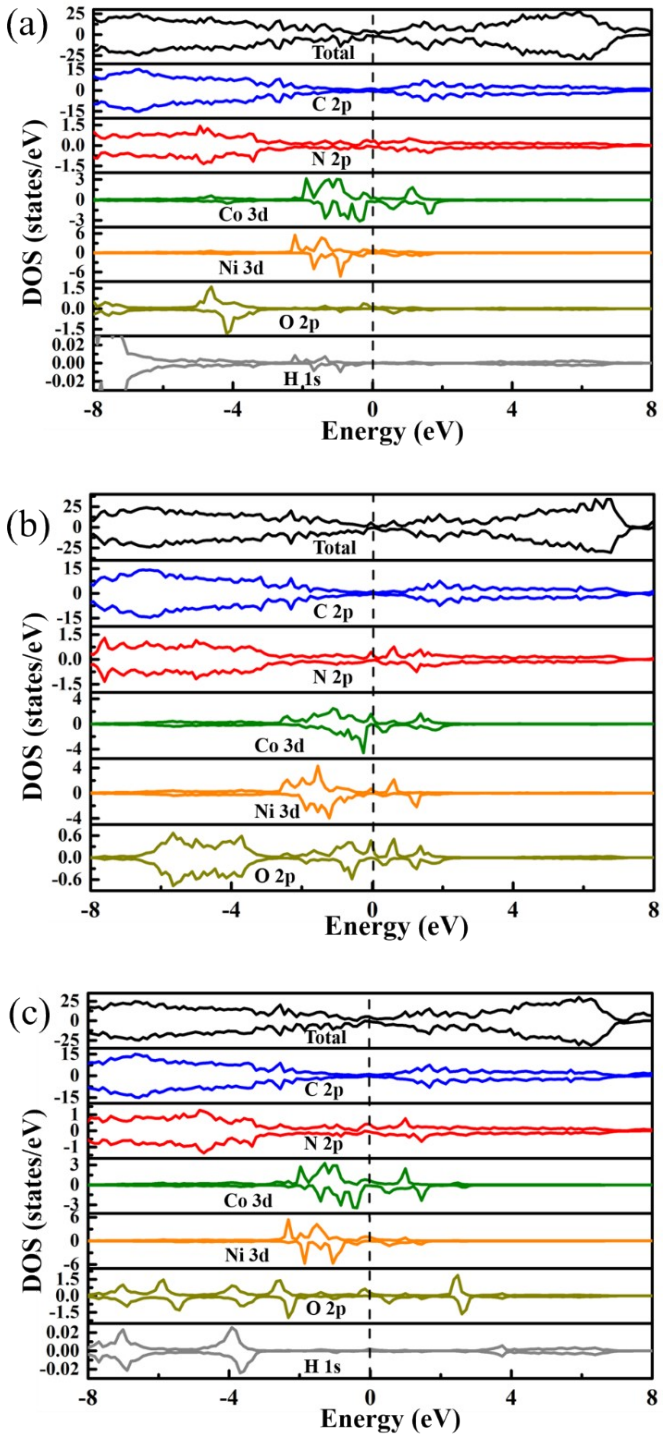

Fig. S20 Spin-polarized density of states for adsorption intermediates (a) OH*, (b) O*, and (c) OOH* on CoNi-N_PG.

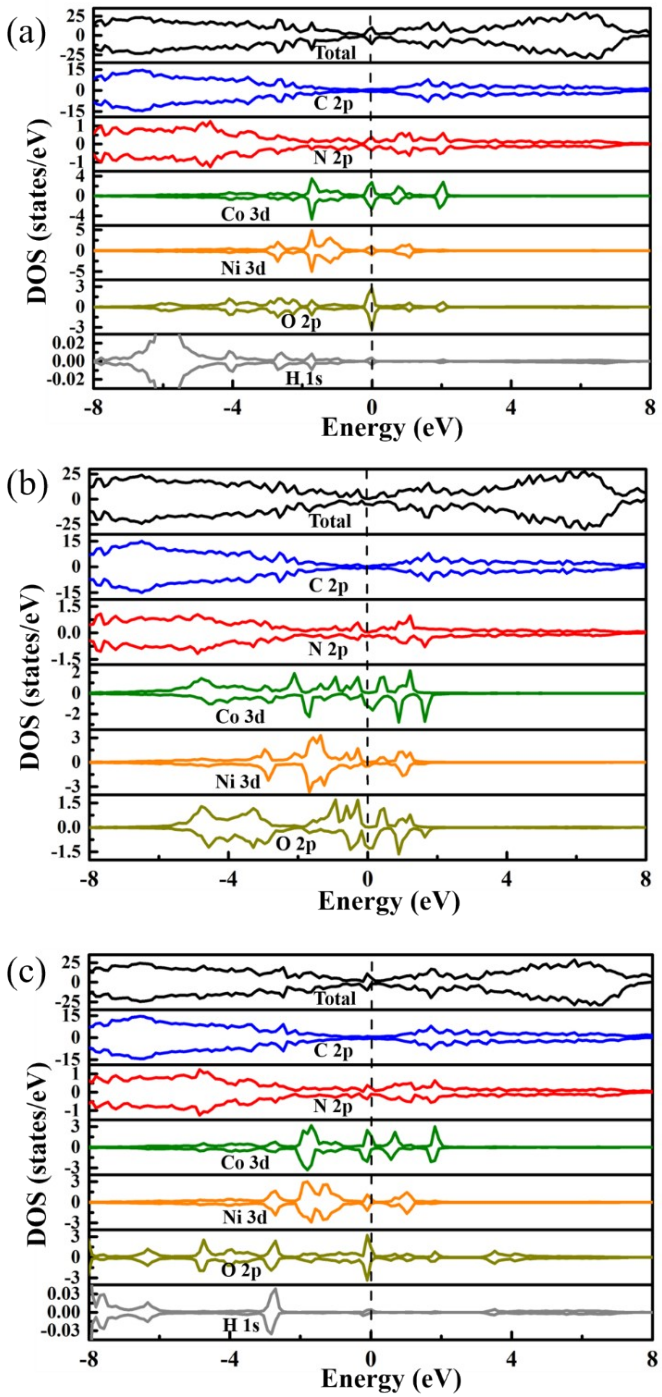

Fig. S21 Spin-polarized density of states for adsorption intermediates (a) OH*, (b) O*, and (c) OOH* on CoNi-N_PG-O.

References

[S1] L. L. Liu, C. P. Chen, L. S. Zhao, Y. Wang and X. C. Wang, *Carbon*, 2017, **115**, 773-780.

[S2] Y. S. Wei, L. Sun, M. Wang, J. Hong, L. Zou, H. Liu, Y. Wang, M. Zhang, Z. Liu and Y. Li, *Angew. Chem. Int. Edit.*, 2020, **132**, 16147-16156.

[S3] L. Ismer, M. S. Park, A. Janotti and C. G. Van de Walle, *Phys. Rev. B*, 2009, **80**, 184110.

[S4] C. G. Van de Walle and J. Neugebauer, *J. Appl. Phys.*, 2004, **95**, 3851-3879.

[S5] E. Finazzi and C. Di Valentin, *J. Phys. Chem. C*, 2007, **111**, 9275-9282.

[S6] S. Kattel, P. Atanassov and B. Kiefer, *Phys. Chem. Chem. Phys.*, 2014, **16**, 13800-13806.

[S7] X. Zheng, Y. Yao, W. Ye, P. Gao and Y. Liu, *Chem. Eng. J.*, 2020, **413**, 128027.

[S8] P. Nematollahi and E. C. Neyts, *Appl. Surf. Sci.*, 2019, **496**, 143618.

[S9] C. Yang, Z. D. Yang, H. Dong, N. Sun, Y. Lu, F. M. Zhang and G. Zhang, *ACS Energy Lett.*, 2019, **4**, 2251-2258.

[S10] H. X. Xu, D. J. Cheng, D. P. Cao and X. C. Zeng, *Nature Catal.*, 2018, **1**, 632-632.

[S11] Q. Zhang, Y. Wang, Y. Wang, A. M. Al-Enizi, A. A. Elzatahry and G. Zheng, *J. Mater. Chem. A*, 2016, **4**, 5713-5718.

[S12] X. Jia, Y. Zhao, G. Chen, L. Shang, R. Shi, X. Kang, G. I. Waterhouse, L. Z. Wu, C. H. Tung and T. Zhang, *Adv. Energy Mater.*, 2016, **6**, 1502585.

[S13] Y. Wang, C. Xie, D. Liu, X. Huang, J. Huo and S. Wang, *ACS Appl. Mater.*

Inter., 2016, **8**, 18652-18657.

[S14] B. Zhang, C. Xiao, S. Xie, J. Liang, X. Chen and Y. Tang, *Chem. Mater.*, 2016, **28**, 6934-6941.

[S15] Y. Wang, B. Zhang, W. Pan, H. Ma and J. Zhang, *ChemSusChem*, 2017, **10**, 4170-4177.

[S16] T. Gao, Z. Jin, Y. Zhang, G. Tan, H. Yuan and D. Xiao, *Electrochim. Acta*, 2017, **258**, 51-60.

[S17] N. T. Suen, S. F. Hung, Q. Quan, N. Zhang, Y. J. Xu and H. M. Chen, *Chem. Soc. Rev.*, 2017, **46**, 337-365.

[S18] T. Liu, M. Li, X. Bo and M. Zhou, *ACS Sustain. Chem. Eng.*, 2018, **6**, 11457-11465.

[S19] Y. Gu, S. Chen, J. Ren, Y. A. Jia, C. Chen, S. Komarneni, D. Yang and X. Yao, *ACS Nano*, 2018, **12**, 245-253.

[S20] L. An, J. Feng, Y. Zhang, Y.-Q. Zhao, R. Si, G.-C. Wang, F. Cheng, P. Xi and S. Sun, *Nano Energy*, 2019, **57**, 644-652.

[S21] M. Lei, Y. Zhang, M. Wang, W. Yang and Z. Gao, *Chem. Eng. J.*, 2021, **421**, 129747.